Korean J. Chem. Eng., **30**(12), 2170-2177 (2013)
DOI: 10.1007/s11814-013-0155-z

pISSN: 0256-1115
eISSN: 1975-7220

Selective catalytic reduction converter design: The effect of ammonia nonuniformity at inlet

Thiyagarajan Paramadayalan*,† and Atul Pant**

*GM Powertrain-India, Engine CAE, GM Tech Center, Bangalore 560066, India
**Global General Motors R&D, India Science Lab, GM Tech Center, Bangalore 560066, India
(*Received 22 May 2013 • accepted 15 August 2013*)

Abstract−A three-dimensional CFD model of SCR converter with detailed chemistry is developed. The model is used to study the effects of radial variation in inlet ammonia profile on SCR emission performance at different temperatures. The model shows that radial variation in inlet ammonia concentration affects the SCR performance in the operating range of 200-400 °C. In automotive SCR systems, ammonia is non-uniformly distributed due to evaporation/reaction of injected urea, and using a 1D model or a 3D model with flat ammonia profile at inlet for these conditions can result in erroneous emission prediction. The 3D SCR model is also used to study the effect of converter design parameters like inlet cone angle and monolith cell density on the SCR performance for a non-uniform ammonia concentration profile at the inlet. The performance of SCR is evaluated using $DeNO_x$ efficiency and ammonia slip.

Key words: Catalytic Converter, SCR Converter, CFD, Numerical Modeling, Monolith Reactor, Chemical Kinetics

INTRODUCTION

Selective catalytic reduction (SCR) using urea is one of the technologies used to reduce NO_x emissions from a diesel automotive exhaust system [1]. In this process, ammonia formed by decomposing urea injected upstream of the SCR converter is used to reduce NO_x in the catalytic converter. Optimal SCR design and operation requires maximizing NO_x reduction efficiency with minimum ammonia slip (i.e., excess ammonia that escapes unreacted). Computer modeling can be used to achieve this goal. Conventionally, 1-D converter models [2,3] based on single channel approach have been used to model SCR performance. These models assume uniform flow, temperature and concentration distribution at the front face of the monolith. This assumption may or may not be applicable for ammonia due to inherent nonuniformity introduced by urea injection and decomposition [4-7]. In addition, heat loss at the external boundary of the converter can change the radial temperature distribution in the converter. Radial flow and temperature variation have to be modeled to accurately predict the converter performance under such conditions.

It is widely established that the performance of an SCR system is strongly influenced by the uniformity of ammonia at SCR inlet [8-10]. Injection and subsequent evaporation of urea solution results in non-uniform ammonia concentration distribution across the monolith face. Several experimental and numerical studies have been performed to optimize the design and operating conditions of injectors to obtain a more uniform NH_3 profile [11-14]. Also, the design of spacers/mixers has been optimized to yield better ammonia concentration uniformity [10,15-17]. The impact of geometric parameters like inlet cone to improve ammonia uniformity has also been studied [18]. However, the role of ammonia flux, i.e., the product of concentration and velocity, has not yet been explored in detail.

There have been some efforts towards modeling the chemical kinetics of NO_x reduction in SCR using computational fluid dynamics (CFD). Karlsson et al. [19] combined the 3D CFD and lumped parameter SCR model, which enables the prediction of system performance with non-uniform exhaust and ammonia profiles. The output of the CFD simulations is fed into the lumped SCR model for evaluation of the overall system performance. Wurzenberger et al. [3] performed a full 3D simulation of an HSO (Hydrolysis-SCR-Oxidizer Catalyst) system considering urea injection and homogeneous gas phase and catalytic reactions. They considered three SCR reactions along with urea conversion reaction. Benjamin and Roberts [20] performed a full CFD study with droplet model for urea injection and SCR reactions on a simple diffuser geometry. Their results indicate that there are limitations to using a spray model as a means to introduce ammonia. Tamaldin et al. [21] did a 3D CFD study with SCR reactions and no urea injection. They used eight reactions for SCR chemistry and also considered the mass transfer between the gas and the solid phase. Experimental data was used to obtain inlet boundary conditions for the CFD model.

Chae et al. [22] modeled the 3-D effects of NH_3 injection on SCR performance. The effect of geometry on the NH_3 concentration profile was obtained by solving a CFD model in CFX. The profile predicted by the CFD model was used as the inlet condition to the reactor model. Further, the study used a simplified SCR kinetics based on pseudo steady state assumption for the coverage of ammonia on catalyst sites.

In the present study, we report the development of a transient CFD model of SCR converter with full SCR chemistry [2]. The SCR reaction model used in this study solves for the transient ammonia coverage on catalyst sites. This improves the model predictions for transient conditions like vehicle drive cycles. The visualization of ammonia coverage distribution inside the monolith can also provide useful insight on the SCR process. Further, to accurately capture the geometry effects, the solution of concentration and flow field is

†To whom correspondence should be addressed.
E-mail: thiyagarajan.paramadayalan@gmail.com

coupled with the reaction kinetics in the CFD model used in this study. This eliminates the need for separately specifying velocity, temperature or concentration profiles at the inlet of the reactor monolith. This model is used to determine the effect of inlet ammonia profile and geometric parameters like cone angle and cell density on the overall NO_x conversion efficiency and ammonia slip. The effect of radial variation in the ammonia concentration at the converter inlet is also determined. Based on this analysis a strategy for an optimum SCR design has been proposed.

SCR MODEL

1. Geometry

A 3.3 liter SCR converter with the specifications listed in Table 1 is used for this study [23]. The converter geometry is symmetrical and hence a 2D axisymmetric model (shown in Fig. 1) is chosen for the analysis. The computational domain contains 7000 hexahedral elements. The mesh elements at the monolith inlet and end of inlet cone are refined further to accurately predict the velocity and temperature distribution along the monolith inlet.

2. Governing Conservation Equations

The computational domain is divided into two regions with the SCR monolith being a porous medium while rest of the domain (inlet/outlet cones and pipes) is modeled as a free flow region. The governing equations are solved using commercial CFD package STARCD [24]. STARCD is a finite volume solver with body-fitted grids. The governing equations are numerically integrated over each of these computational cells or control volumes. The grids are non-staggered and all variables are evaluated at cell centers.

Table 1. Monolith properties

Material	Cordierite
Monolith length (mm)	203
Monolith diameter (mm)	144
Inlet pipe diameter (mm)	56
Cone length (mm)	77
Cell density (cpsi)	400
Substrate thickness (mil)	4.3
Washcoat loading (g/l)	110
Zeolite site density (mol-site)/m^3	200

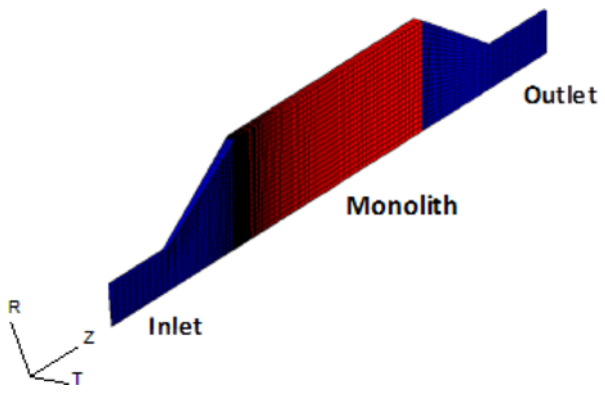

Fig. 1. 2D Axisymmetric model. Red zone is the monolith (porous medium) and blue zones are the inlet and outlet cones.

2-1. Free Flow Region Outside Monolith

In the free flow region, Reynolds averaged governing equations for mass, momentum, energy and species mass conservation are solved in cylindrical coordinates (z, r, θ). 2D axisymmetric model in star-CD represents a 5 degree slice of original 3D model and the assumption of axisymmetry implies that there are no gradients in the circumferential (θ) direction.

Mass conservation equation,

$$\frac{\partial \rho}{\partial t}+\frac{\partial}{\partial z}(\rho u)+\frac{1}{r}\frac{\partial}{\partial r}(r\rho v)=0 \tag{1}$$

Momentum equations in axial, radial and tangential directions are as follows:

$$\frac{\partial(\rho u)}{\partial t}+\frac{\partial}{\partial z}(\rho uu)+\frac{1}{r}\frac{\partial}{\partial r}(r\rho vu)=-\frac{\partial p}{\partial z}+F_z+2\frac{\partial}{\partial z}\left(\mu_{eff}\frac{\partial u}{\partial z}\right)+\frac{1}{r}\frac{\partial}{\partial r}\left[r\mu_{eff}\left(\frac{\partial u}{\partial r}+\frac{\partial v}{\partial z}\right)\right]-\frac{2}{3}\frac{\partial}{\partial z}\left[\mu_{eff}\left(\frac{\partial u}{\partial z}+\frac{1}{r}\frac{\partial(rv)}{\partial r}\right)\right] \tag{2}$$

$$\frac{\partial(\rho v)}{\partial t}+\frac{\partial}{\partial z}(\rho uv)+\frac{1}{r}\frac{\partial}{\partial r}(r\rho vv)=-\frac{\partial p}{\partial r}+F_z+\frac{2}{r}\frac{\partial}{\partial r}\left(r\mu_{eff}\frac{\partial v}{\partial r}\right)+\frac{\partial}{\partial z}\left[\mu_{eff}\left(\frac{\partial u}{\partial r}+\frac{\partial v}{\partial z}\right)\right]-\mu_{eff}\frac{2v}{r^2}-\frac{2}{3}\frac{\partial}{\partial z}\left[\mu_{eff}\left(\frac{\partial u}{\partial z}+\frac{1}{r}\frac{\partial(rv)}{\partial r}\right)\right]+\rho\frac{w^2}{r} \tag{3}$$

$$\frac{\partial(\rho w)}{\partial t}+\frac{\partial}{\partial z}(\rho uw)+\frac{1}{r}\frac{\partial}{\partial r}(r\rho vw)=\frac{\partial}{\partial z}\left(\mu_{eff}\frac{\partial w}{\partial z}\right)+\frac{1}{r}\frac{\partial}{\partial r}\left[r\mu_{eff}\frac{\partial w}{\partial z}\right]-\rho\frac{vw}{r}-\frac{w}{r^2}\frac{\partial}{\partial r}(r\mu_{eff}) \tag{4}$$

In the above equations, u, v and w are time averaged axial, radial and circumferential velocity components, respectively; p is pressure, ρ is density and μ_{eff} is effective viscosity, with contribution from laminar and turbulent components,

$$\mu_{eff}=\mu_l+\mu_t \quad \text{with} \quad \mu_t=\frac{\rho C_\mu k^2}{\varepsilon} \tag{5}$$

The energy equation is expressed in terms of gas phase enthalpy (h_f),

$$\frac{\partial(\rho h_f)}{\partial t}+\frac{\partial}{\partial z}(\rho u h_f)+\frac{1}{r}\frac{\partial}{\partial r}(r\rho v h_f)=\frac{\partial}{\partial z}\left(\left(\frac{k}{C_p}+\frac{\mu_t}{\sigma_t}\right)\frac{\partial h_f}{\partial z}\right)+\frac{1}{r}\frac{\partial}{\partial r}\left[r\left(\frac{k}{C_p}+\frac{\mu_t}{\sigma_t}\right)\frac{\partial h_f}{\partial r}\right] \tag{6}$$

where k is thermal conductivity, C_p is specific heat at constant pressure and σ_t is the Prandtl number. The species mass conservation equation is given as follows:

$$\frac{\partial(\rho x_g)}{\partial t}+\frac{\partial}{\partial z}(\rho u x_g)+\frac{1}{r}\frac{\partial}{\partial r}(r\rho v x_g)=\frac{\partial}{\partial z}\left(\Gamma_c\frac{\partial x_g}{\partial z}\right)+\frac{1}{r}\frac{\partial}{\partial r}\left(r\Gamma_c\frac{\partial x_g}{\partial r}\right) \tag{7}$$

The turbulence in the flow along the cone region is accounted for using a RNG k-ε model. Turbulent kinetic energy (k) and dissipation rate (ε) equations are given in Eqs. (8) and (9). The turbulence constants can be found at [25].

$$\frac{\partial(\rho k)}{\partial t}+\frac{\partial}{\partial z}(\rho uk)+\frac{1}{r}\frac{\partial}{\partial r}(r\rho vk)=\frac{\partial}{\partial z}\left[\alpha_k\mu_{eff}\frac{\partial k}{\partial z}\right]$$

$$+\frac{1}{r}\frac{\partial}{\partial r}\left[r\alpha_k\mu_{eff}\frac{\partial k}{\partial r}\right]+G-\rho\varepsilon \tag{8}$$

$$\frac{\partial(\rho\varepsilon)}{\partial t}+\frac{\partial}{\partial z}(\rho u\varepsilon)+\frac{1}{r}\frac{\partial}{\partial r}(r\rho v\varepsilon)=\frac{\partial}{\partial z}\left[\alpha_k\mu_{eff}\frac{\partial\varepsilon}{\partial z}\right]+\frac{1}{r}\frac{\partial}{\partial r}\left(r\alpha_k\mu_{eff}\frac{\partial\varepsilon}{\partial r}\right)+\frac{\varepsilon}{k}(C_1G-\rho C_2\varepsilon-R) \tag{9}$$

$$G=\mu_t\left\{2\left[\left(\frac{\partial u}{\partial z}\right)^2\right]+\left(\frac{\partial v}{\partial r}\right)^2+\left(\frac{v}{r}\right)^2+\left(\frac{\partial w}{\partial r}-\frac{w}{r}\right)^2+\left(\frac{\partial w}{\partial z}\right)^2+\left(\frac{\partial v}{\partial z}+\frac{\partial u}{\partial r}\right)^2\right\} \tag{10}$$

$$R=\frac{C_\mu\rho\eta^3(1-\eta/\eta_0)\varepsilon}{1+\beta\eta^3} \tag{11}$$

where,

η_0=4.38, β=0.012 and $\eta\equiv Sk/\varepsilon$, S being the modulus of mean rate of strain, which is related to G as, $S=\sqrt{G/\mu_t}$

2-2. Flow Inside Monolith

The flow field inside the monolith is assumed to be fully developed and laminar. Star-CD solves the pressure drop in the porous domain as an additional source term in the momentum equation as follows:

$$K_i v_i=\frac{\partial p}{\partial \xi_i} \tag{12}$$

The porous resistance K_i is assumed to be a function of the superficial velocity magnitude |v| of the form

$$K_i=\alpha_i|v|+\beta_i \tag{13}$$

where α_i and β_i are resistance coefficients calculated from monolith characteristics given by Kays [26],

$$\alpha_i=\frac{\rho}{2L\chi^2}(K_c+K_e)\qquad \beta_i=\frac{2f_{shape}\mu}{\chi D_h^2} \tag{14}$$

The calculated α_i and β_i are specified only in the axial direction because the flow in the monolith channels is unidirectional. The transverse α_i is set to zero and β_i is assigned large values (10^8) to suppress the flow in radial directions [27].

The energy equations in both fluid and solid domains of the monolith are solved using the conjugate heat transfer between the two domains represented via a source term. Porous medium energy balance is given as follows:

$$\chi\rho C_p\frac{\partial T_g}{\partial t}+\rho\frac{\partial}{\partial z}(u_sT_g)+\rho\frac{1}{r}\frac{\partial}{\partial r}(rv_sT_g)=\frac{\partial}{\partial z}\left[k_{eff}\frac{\partial T_g}{\partial z}\right]+\frac{1}{r}\frac{\partial}{\partial r}\left[k_{eff}r\frac{\partial T_g}{\partial r}\right]-hS(T_g-T_s) \tag{15}$$

The final term in Eq. (16) gives the heat transfer between gas and substrate. Gas density ρ is a function of temperature based on ideal gas law. The solid phase energy equation inside the substrate is given as follows:

$$(1-\chi)C_{ps}\rho_s\frac{\partial T_s}{\partial t}=\frac{\partial}{z}\left(k_{z,eff}\frac{\partial T_s}{\partial z}\right)+\frac{1}{r}\frac{\partial}{\partial r}\left(k_{r,eff}\frac{\partial T_s}{\partial r}\right)+hS(T_g-T_s)-\sum_{j=1}^{nrct}\eta_j a_j(z)(\Delta H)_j R_j \tag{16}$$

Species transport equation inside the monolith:

$$\frac{\partial(\chi\rho x_g)}{\partial t}+\frac{\partial}{\partial z}(\rho u_s x_g)+\frac{1}{r}\frac{\partial}{\partial r}(r\rho v_s x_g)=\frac{\partial}{\partial z}\left(\Gamma_c\frac{\partial x_g}{\partial z}\right)+\frac{1}{r}\frac{\partial}{\partial r}\left(r\Gamma_c\frac{\partial x_g}{\partial r}\right)+k_{mi}S(x_{g,i}-x_{s,i}) \tag{17}$$

The mass transfer between gas to the substrate surface is solved as an algebraic differential equation:

$$-k_{m,i}S(x_{g,i}-x_{s,i})=\sum_{j=1}^{nrct}\eta_j a_j(z)s_{ij}R_j\qquad i=1, 2..nsp \tag{18}$$

And coverage is solved with a transport equation with no convective and diffusion terms and only with a source term as follows:

$$\frac{\partial\theta}{\partial t}=\sum_{j=1}^{nrct}\eta_j s_{\theta j}R_j \tag{19}$$

3. Chemical Reaction Kinetics

The reaction chemistry is based on the mechanism proposed by Olsson et al. [2] The reactions and rate expressions are shown Table 2. The kinetic rate constants obtained by Olsson et al. [2] are directly used in the CFD model calculations.

4. Boundary Conditions

Transient simulations are performed with 20 g/s and 100 g/s of inlet feed flow rate consisting of 200 ppm of NH_3 and NO. Simulations are carried out assuming both flat and parabolic profiles for the ammonia concentration distribution across the inlet pipe, while the inlet velocity is represented with a flat profile. A parabolic profile choice adequately represents the radial variations of urea concentra-

Table 2. SCR reaction chemistry [2]

#	Reaction	Rate Expression
1. NH_3 Adsorption/Desorption	$NH_3+\sigma\leftrightarrows NH_3\text{-}\sigma$	$K_{1,f}C_{NH_3}(1-\theta_{NH_3})-K_{1,b}\,\theta_{NH_3}$
2. NH_3 Oxidation	$2NH_3+1.5O_2\rightarrow N_2+3H_2O+2\,\sigma$	$K_2\,C_{O_2}\,\theta_{NH_3}$
3. NO Oxidation	$NO+0.5O_2\leftrightarrows NO_2$	$K_{3,f}(C_{O_2})^{0.5}\,C_{NO}-K_{3,b}\,C_{NO_2}{}^a$
4. Standard SCR	$4NH_3\text{-}\sigma+4NO+O_2\rightarrow 4N_2+6H_2O+4\,\sigma$	$K_4\,C_{NO}\,\theta_{NH_3}$
5. Fast SCR	$2NH_3\text{-}\sigma+NO+NO_2\rightarrow 2N_2+3H_2O+2\,\sigma$	$K_5\,C_{NO}\,C_{NO_2}\,\theta_{NH_3}$
6. Slow SCR	$4NH_3\text{-}\sigma+NO_2\rightarrow 3.5N_2+6H_2O+4\,\sigma$	$K_6\,C_{NO_2}\,\theta_{NH_3}$
7. N_2O formation	$2NH_3\text{-}\sigma+2NO_2\rightarrow N_2+N_2O+3H_2O+2\,\sigma$	$K_7\,C_{NO_2}\,\theta_{NH_3}$

[a] $K_{3,b}$ is calculated from the thermodynamic restrictions

The rate constant K is calculated using, $K=A\,e_A^{-[E/RT]}$

tion as a result of urea injection from the pipe wall. For the parabolic profile approximation, the NH_3 concentration is calculated using the formula $C=C_{max}(1-r^2/R^2)$, where C_{max} is the maximum ammonia concentration near the axis. The SCR performance is established at five different inlet temperatures ranging from 150 to 550 °C. The pressure at the SCR outlet is fixed at atmospheric pressure. Converter walls are subjected to heat loss boundary conditions with Nusselt number calculated from the following formula [28]:

$$Nu=(0.6+0.387(GR.Pr)^{1/6}/(1+0.559/Pr)^{9/16})^{8/27})^2 \quad (20)$$

Typical heat transfer coefficient values are 10 W/m^{2}K for the monolith region and 20 W/m^{2}K for the cone region. The initial bed temperature is fixed at 300 K.

5. Numerical Procedure

The model is simulated until NH_3 and NO concentration at the outlet reaches a steady state. Numerical results of flow distribution, velocity profile and NH_3, NO, NO_2, N_2O profiles at different temperatures are obtained using this model. For all the simulations, performance of SCR is measured in terms of the $DeNO_x$ efficiency and ammonia slip. $DeNO_x$ efficiency is defined as the NO_X conversion across the SCR given by Eq. (21). The ammonia concentration at the outlet is calculated as flux weighted average across the outlet. Ammonia slip is the amount of unconverted ammonia leaving the SCR.

$$DeNO_x=\frac{NO_x\ in-NO_x out}{NO_x\ in} \quad (21)$$

In addition, the uniformity index (UI) defined by Eqs. (22) and (23) is calculated to characterize the flow and concentration non-uniformity at SCR inlet. In these equations, φ is the parameter for which uniformity index is calculated. It is general practice to use concentration based uniformity i.e. $\phi=x_g$, but in this paper φ is based on the net species flux, $\phi=\rho u x_g$.

$$UI=1-\frac{\int|\phi-\bar{\phi}|\cdot dA}{2\bar{\phi}A} \quad (22)$$

$$\bar{\phi}=\frac{\int\phi\cdot dA}{A} \quad (23)$$

To differentiate the effects of flux based uniformity (φ) over concentration uniformity (x_g), both the parameters are used in the study and labeled as "NH_3-flux" and "NH_3-conc", respectively, in the results section. In addition to the CFD model, a 1D SCR model described by Olsson et al. [2] is also simulated for the conditions described above. The results from the CFD and 1D model are compared to establish the presence and magnitude of the 3D effects.

EXPERIMENTAL VALIDATION

The model has been validated using experimental data obtained on a flow reactor test. A catalyst sample with length 30 mm and diameter 22 mm was used in the reactor. The flow rate of the gas was 6.63e-5 kg/s and the concentrations were 500 ppm for ammonia, 500 ppm for NO and 8% O2. A stepwise increment of temperature was applied from 100 to 500 °C with 50 °C increment for every 20 min. The experiments were conducted for a total duration of 250 min. Different phases of SCR reactor like NH_3 adsorption/desorption, NO reduction/oxidation and NH_3 oxidation were observed. The model results are in close in close agreement with the experimental values as shown in Fig. 2 and 3.

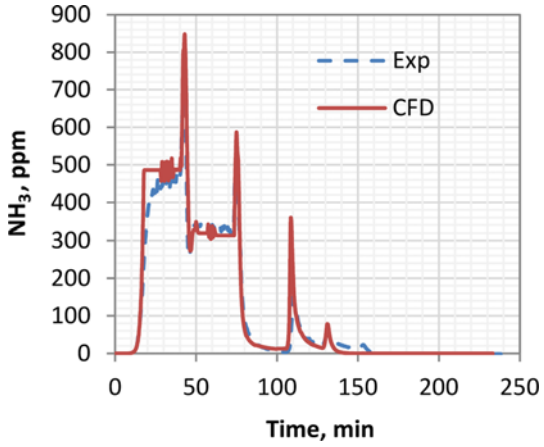

Fig. 2. Measured and calculated NH_3 concentration (ppm) at SCR outlet during NH_3 SCR experiment.

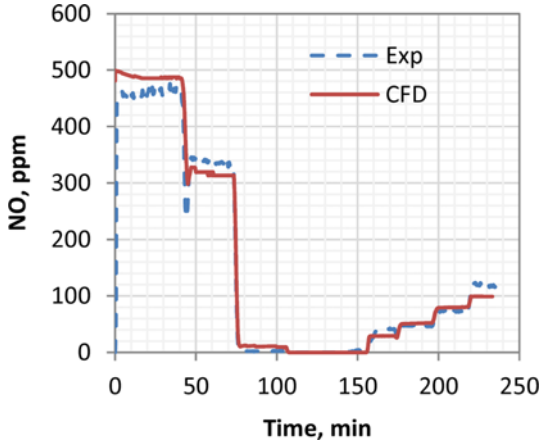

Fig. 3. Measured and calculated NO concentration (ppm) at SCR outlet during NH_3 SCR experiment.

RESULTS AND DISCUSSION

The validated model is used to study the effect of radial non-uniformity in inlet ammonia concentration and the geometric design factors on SCR performance. The results from those simulations are discussed in this section.

1. Effect of NH_3 Profile Along the Inlet

Fig. 4 shows the $DeNO_x$ efficiency at different temperatures. As expected, the efficiency is maximum at an intermediate temperature range of (250-350 °C) [29]. At a lower temperature (150 °C), the efficiency decreases due to lower reaction rates; whereas at higher temperatures (above 350 °C) the efficiency decreases due to increased oxidation of ammonia. The corresponding ammonia slip at the converter outlet is shown in Fig. 5. Most of the ammonia leaves the SCR unconverted at the lower temperature. Figs. 4 and 5 also include the 1D model and CFD model results obtained for a flat ammonia profile at the inlet. The results show that in the absence of a radial variation in ammonia, the 1D model results are in agreement with

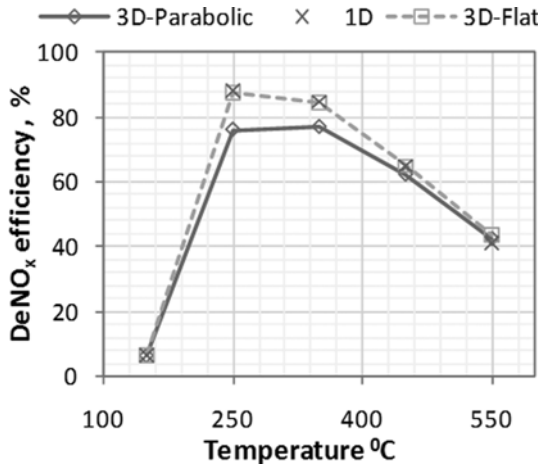

Fig. 4. DeNO$_x$ Efficiency. The DeNO$_x$ efficiency is calculated at different temperatures for the three models: (a) CFD with parabolic profile, (b) CFD with flat profile and (c) 1D model.

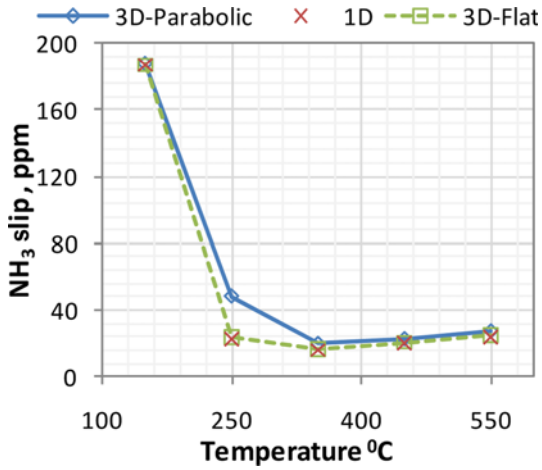

Fig. 5. NH$_3$ Slip (ppm) at the outlet. NH$_3$ slip is calculated at the outlet of converter at different temperatures for the three models: (a) CFD with parabolic profile, (b) CFD with flat profile and (c) 1D model.

the CFD model results. However, using a parabolic ammonia profile a significant variation (≈10% on NO$_x$ conversion efficiency) is observed at intermediate temperatures. But at low and high temperatures, all three models predict similar NO$_x$ conversion and ammonia slip. This implies that using a 1D model to describe SCR performance at intermediate temperatures will give misleading results because the effect of radial variation in ammonia profile will not be predicted accurately.

A comparison of NO and NH$_3$ contours in Figs. 6 and 7, respectively, shows that radial variations in the concentrations exist at all temperatures. Due to the higher ammonia concentration more NO conversion occurs near the axis. However, this radial variation does not have a significant impact on the overall conversion at extreme temperatures (150 and 550 °C). This observation can be explained by comparing the NH$_3$ coverage (i.e., the fraction of NH$_3$ sites occupied in the catalyst) contours (Fig. 8). At 150 °C and 550 °C, the ammonia coverage fraction is the same throughout the SCR. At the lower or higher temperatures the following effect is seen. At 150 °C

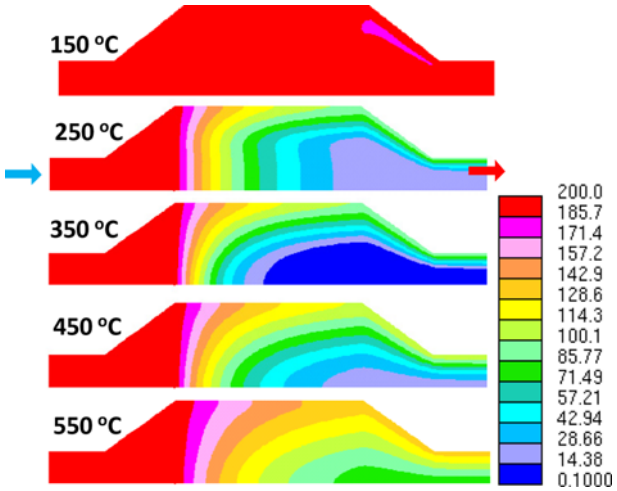

Fig. 6. NO Contours (ppm). Steady state NO contours at different operating temperature parabolic NH$_3$ profile at inlet.

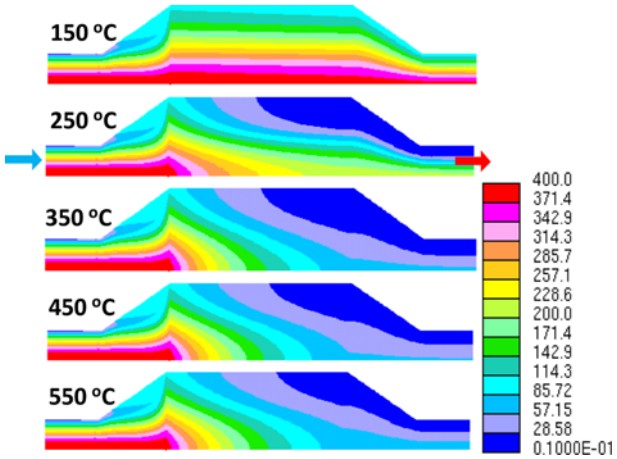

Fig. 7. NH$_3$ Contour (ppm). Steady state NH$_3$ profiles for different operating temperatures with parabolic NH$_3$ profile at inlet.

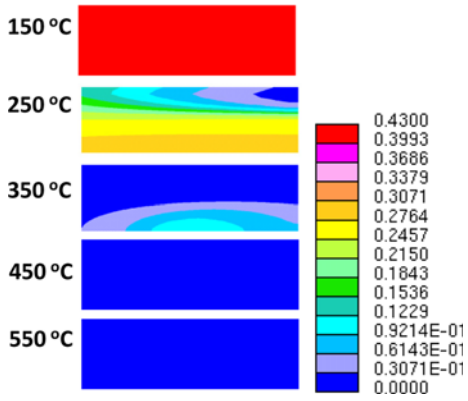

Fig. 8. NH$_3$ Coverage. Steady state coverage fraction inside the monolith for different temperatures with parabolic NH$_3$ profile at inlet.

all the catalyst sites are saturated with ammonia, and at 550 °C all the adsorbed ammonia is readily oxidized. This lowers the impact of any radial variation in ammonia concentration on the final con-

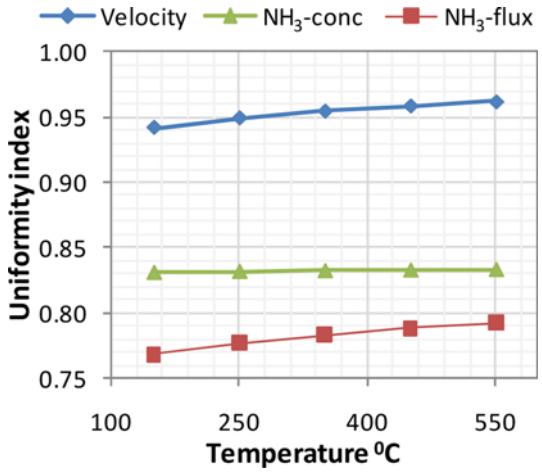

Fig. 9. Uniformity index. Change in velocity and NH_3 uniformity index values with temperature for the CFD model with parabolic NH_3 profile. Please refer to Eq. (22) for the definition.

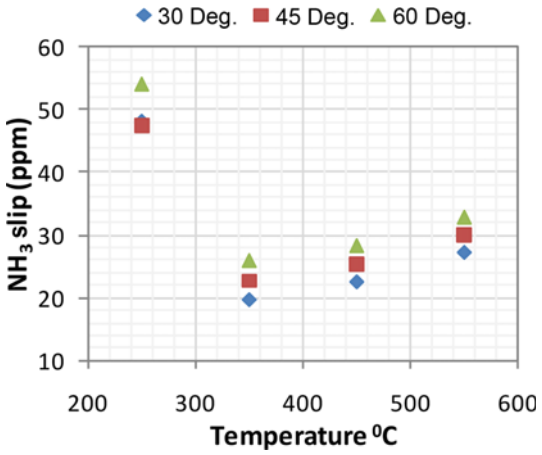

Fig. 11. Steady state ammonia slip for different cone angles as a function of inlet temperature.

version since all the SCR reaction rates depend on ammonia stored on the catalyst [2]. In addition, the flow uniformity at the SCR inlet increases with temperature (due to higher velocity and pressure drop inside monolith) (Fig. 9), which further reduces the radial variations at higher temperature. At intermediate temperatures, SCR reaction rates are comparable to ammonia adsorption-desorption and oxidation, and therefore the radial variation in ammonia reduces NO_x conversion. Also, both the radial and axial variation in temperature inside the monolith is very minimal since the SCR reactions are not exothermic as reported by Olsson et al. [2] Therefore, the effect of radial and axial temperature variation on ammonia coverage can be neglected. For the case of flat ammonia profile assumption across the inlet, the NO, NH_3 concentration and NH_3 coverage show negligible radial variations inside the monolith, and the CFD results are very close to the 1D model results.

2. Effect of Converter Geometry

The CFD model is used to study the effect of converter geometry on SCR performance. The geometry discussed in the previous section is chosen as the base case. The SCR performance for varying 1) inlet cone angle (θ) and 2) monolith cell density (CPSI) has been established.

2-1. Effect of Cone Angle

The SCR performance in converters with 30, 45 and 60 degree cone angles was studied using our model. In these converter geometries the inlet cone length was varied while the inlet pipe and the monolith diameter were kept constant. Figs. 10 and 11 show the change in $DeNO_X$ efficiency and NH_3 slip, respectively, at different cone angles. A marginal improvement in SCR performance is observed at smaller cone angles. As the cone angle increases, the monolith comes closer to the inlet pipe, reducing the distance available for flow to expand. This leads to a slight decrease in flow uniformity as seen from Fig. 12, and hence a decrease in SCR performance.

2-2. Effect of CPSI

The effect of channel cell density on the SCR performance is determined using the base case converter geometry specified in Table 1. The cell density and corresponding substrate thickness [30,31] used in the SCR models are shown in Table 3. Figs. 13 and 14 show that the $DeNO_X$ efficiency and ammonia slip, respectively, do not change significantly with cell density. There is a minor improvement in SCR performance at higher cell density. Increase in inter-

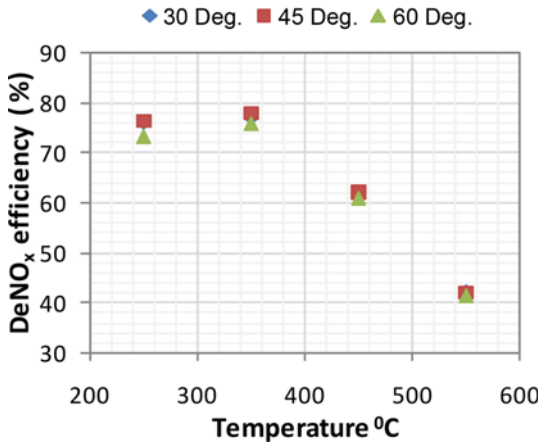

Fig. 10. Steady state $DeNO_x$ efficiency for different cone angles as a function of inlet temperature.

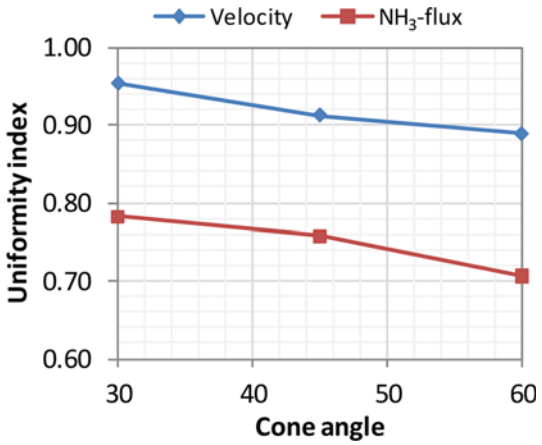

Fig. 12. Velocity and NH_3 uniformity index change for different cone angles as a function of inlet temperature.

Table 3. Variation of monolith geometric parameters with cell density

CPSI	Substrate thickness (mil)	Washcoat thickness (mil)	Geometric surface area (m^2/m^3)	Volume porosity	Hydraulic diameter, mm
300	6.5	1.44	2284	0.70	1.23
400	4.3	1.20	2727	0.75	1.10
600	2.5	0.96	3439	0.80	0.93
900	2.5	0.80	4144	0.77	0.75

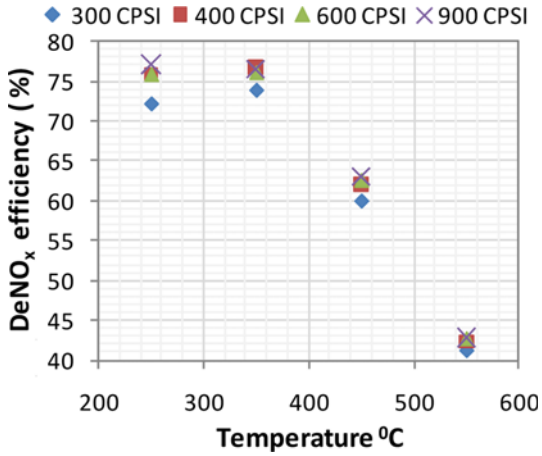

Fig. 13. Steady state $DeNO_x$ efficiency for different cell density values as a function of inlet temperature.

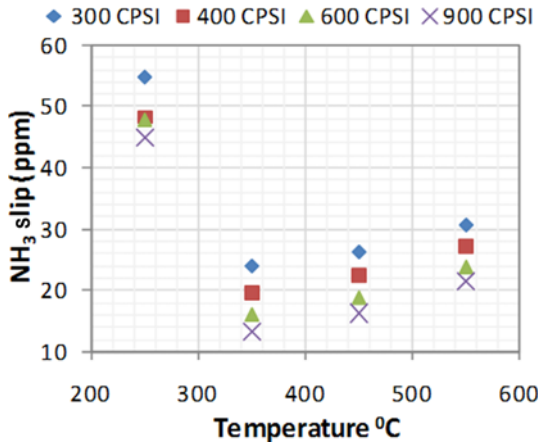

Fig. 14. Steady state ammonia slip for different cell density values as a function of inlet temperature.

face area at higher cell density will enhance the mass transfer from the gas to the catalyst surface. This increase only has a small effect indicating that the SCR reactions are not limited by mass transport as reported by Olsson et al. [2].

SUMMARY

A CFD model of SCR converter is developed with detailed SCR chemistry. The resulting model takes into account all the radial variations at the monolith inlet, gas-solid heat and mass transfer as well as the chemical reactions in a typical SCR. The model is used to establish the SCR performance for different radial variations in inlet ammonia profile. In the absence of radial variations in inlet concentration, the SCR performance predicted by the CFD model is in close agreement with the 1D model. However, in the presence of radial variations the 1D model will over-predict the $DeNO_x$ efficiency.

It is also shown that the radial effects significantly reduce the SCR performance if the ammonia concentration at the converter inlet is non-uniform. Reducing the radial non-uniformity of the ammonia which is formed by urea injection and its decomposition can significantly improve the SCR performance. The uniformity factor based on ammonia flux rather than only the concentration is a better indicator of the effect of radial non-uniformity on the SCR performance.

The CFD model is used to explore the effect of changing converter geometry to improve the SCR performance in case of a parabolic inlet ammonia concentration. In all the geometric configurations tested, the SCR performance does not reach the level obtained using a flat ammonia profile. The change in inlet cone angle of the converter as well as the monolith cell density does not have a significant effect on the SCR performance.

NOMENCLATURE

Cp_s : specific heat capacity of substrate [J/kg/K]
aj(z) : active site density for jth reaction [mol-site(cat)/m^3]
D_h : hydraulic diameter [m]
D_i : diffusivity of gas [m^2/s]
f_{shape} : friction shape factor
Gr : Grashof number
h_f : gas phase enthalpy [J/kgK]
h : heat transfer coefficient [w/m^2K]
K : turbulent kinetic energy [m^2/s^2]
K_c : entrance pressure loss coefficient
K_e : exit pressure loss coefficient
k_{eff} : effective gas phase conductivity [W/mK]
K_g : thermal conductivity of gas [W/mK]
$K_{z,eff}$: axial thermal conductivity of substrate [W/mK]
$K_{r,eff}$: radial thermal conductivity of solid [W/mK]
K_{mi} : mass transfer coefficient [m/s]
L : length of monolith [m]
Nu : nusselt number
nsp : number of reacting species
nrct : number of reactions
P : operating pressure
Pr : Prandtl number [Pa]
R_j : specific reaction rate for j^{th} reaction or turnover rate [mol/mol-site(cat)/sec]
S : surface area of substrate per converter volume [m^2/m^3]
S_{ij} : stoichiometric coefficient of ith species in jth reaction
$S_{\theta j}$: stoichiometric coefficient of adsorbed NH_3 in jth reaction
T : temperature [K]
Ts : solid phase temperature [K]
T_g : fluid temperature [K]
t : time [seconds]
u_s,v_s : superficial velocity [m/s]
x, y, z : axis direction

X_g : mass fraction of species in gas phase
X_s : mass fraction of species in solid phase

Greek Symbols

ΔH_j : heat of reaction for reaction J [J/mol]
μ : viscosity of gas [kg/ms]
η_j : effectiveness factor for the j^{th} reaction
ρ : density of gas [Kg/m^3]
σ_h : turbulent prandtl number
Φ : species mass flux [Kg/m^2s]
θ_k : coverage parameter for the k^{th} storage
Γ_c : species mass diffusivity [m^2/s]
χ : volume porosity

REFERENCES

1. C. Lambert, R. Hammerle, R. McGill, M. Khair and C. Sharp, *Technical advantages of urea SCR for light-duty and heavy-duty diesel vehicle applications*, SAE 2004-01-1292 (2004).
2. L. Olsson, H. Sjövall and R. J. Blint, *Appl. Catal. B: Environ.*, **81**, 203 (2008).
3. J. C. Wurzenberger and R. Wanker, *Multi-scale SCR modeling, 1D kinetic analysis and 3D system simulation*, SAE 2005-01-0948 (2005).
4. X. Zhang and M. Romzek, *Computational fluid dynamics (CFD) applications in vehicle exhaust system*, SAE 2008-01-0612 (2008).
5. S.-J. Jeong, S.-J. Lee, W.-S. Kim and C. B. Lee, *Simulation on the optimum shape and location of urea injector for urea-SCR system of heavy-duty diesel engine to prevent NH_3 slip*, SAE 2005-01-3886.
6. M. Koebel, M. Elsener and M. Kleemann, *Catal. Today*, **59**, 335 (2000).
7. S. D. Yim, S. J. Kim, J. H. Baik, I.-S. Nam, Y. S. Mok, J.-H. Lee, B. K. Cho and S. H. Oh, *Decomposition of urea into NH_3 for the SCR process*, *American Chemical Society*, **43**, 4856 (2004).
8. T. L. McKinley, A. G. Alleyne and C.-F. Lee, *Mixture non-uniformity in SCR systems: Modeling and uniformity index requirements for steady-state and transient operation*, SAE 2010-01-0883 (2010).
9. Å. Johansson, U. Wallin, M. Karlsson, A. Isaksson and P. Bush, *Investigation on uniformity indices used for diesel exhaust aftertreatment systems*, SAE 2008-01-0613 (2008).
10. G. Zheng, G. Palmer, G. Salanta and A. Kotrba, *Mixer development for urea SCR applications*, SAE 2009-01-2879 (2009).
11. X. Zhang and M. Romzek, *3-D numerical study of flow mixing in front of SCR for different injection systems*, SAE 2007-01-1578 (2007).
12. I. Cho, S. Lee, H. Kang and D. S. Baik, *A study on the NO_x reduction of urea-selective catalytic reduction (SCR) system in a heavy-duty diesel engine*, SAE 2007-01-3447 (2007).
13. S.-J. Jeong, S.-J. Lee, W.-S. Kim and C. B. Lee, *Simulation on the optimum shape and location of urea injector for urea-SCR system of heavy-duty diesel engine to prevent NH_3 slip*, SAE 2005-01-3886 (2005).
14. van R. Helden, R. Verbeek, F. Willems and R. vander Welle, *Optimization of urea SCR deNO_x systems for HD diesel engines*, SAE 2004-01-0154 (2004).
15. P. Way, K. Viswanathan, P. Preethi, A. Gilb, N. Zambon and J. Blaisdell, *SCR performance optimization through advancements in aftertreatment packaging*, SAE 2009-01-0633 (2009).
16. Y. Yi, *Development of a 3D numerical model for predicting spray, urea decomposition and mixing in SCR systems*, SAE 2007-01-3985 (2007).
17. M. Chen and S. Williams, *Modelling and optimization of SCR-exhaust aftertreatment systems*, SAE 2005-01-0969 (2005).
18. X. Zhang, T. Gomulka and M. Romzek, *Numerical optimization of flow uniformity inside an F-oval substrate*, SAE 2007-01-1088 (2007).
19. M. Karlsson, U. Wallin, S. Fredholm, J. Jansson, G.-O. Wahlström, C. M. Schär, C. H. Onder and L. Guzzella, *A Combined 3D/lumped modeling approach to ammonia SCR after-treatment systems: Application to mixer designs*, SAE 2006-01-0469 (2006).
20. S. F. Benjamin and C. A. Roberts, *The porous medium approach applied to CFD modelling of SCR in an automotive exhaust with injection of urea droplets*, in IMechE Conference Internal Combustion Engines: Performance, Fuel Economy and Emissions, London (2007).
21. N. Tamaldin, C. A. Roberts and S. F. Benjamin, *Experimental study of SCR in a light-duty diesel exhaust to provide data for validation of a CFD model using the porous medium approach*, SAE 2010-01-1177 (2010).
22. H. J. Chae, S. T. Choo, H. Choi, I.-S. Nam, H. S. Yang and S. L. Song, *Ind. Eng. Chem. Res.*, **39**, 1159 (2000).
23. A. Frobert, Y. Creff, S. Raux, C. Charial, A. Audouin and L. Gagnepain, *SCR for passenger car: Ammonia-storage issue on a Fe-ZSM5 catalyst*, SAE 2009-01-1929 (2009).
24. STAR-CD, *STAR-CD Users Guide and Methodology, version 4.12*, Computational Dynamics Ltd. (2010).
25. V. Yakhot, S. A. Orszag, S. Thangam, T. B. Gatski and C. G. Speziale, *Phys. Fluids A: Fluid Dynamics*, **4**, 1510 (1992).
26. W. M. Kays and W. Morrow, *Compact heat exchangers*, McGraw-Hill Book Company (1964).
27. S.-J. Jeong and W.-S. Kim, *Chem. Eng. Process.*, **42**, 879 (2003).
28. J. Breuer, R. Brück, R. Diewald and P. Hirth, *Temperature examinations on a metal catalyst system*, SAE 971028 (1997).
29. K. Narayanaswamy and Y. He, *Modeling of copper-zeolite and iron-zeolite selective catalytic reduction (SCR) catalysts at steady state and transient conditions*, SAE 2008-01-0615 (2008).
30. K. W. Hughes, D. Gian and J. Calleja, *Relative benefits of various cell density ceramic substrates in different regions of the FTP cycle*, SAE 2006-01-1065 (2006).
31. S. C. Lauderdale, S. T. Nickerson, J. D. Pesansky and C. M. Sorensen, *Impact of ceramic substrate web thickness on emission light-off, pressure drop, and strength*, SAE 2008-01-0808 (2008).